# Fluid inclusion constraints on the genesis of the Puladi muscovite deposit in Gongshan County, Yunnan Province

**Qiong YIN Wei LIU**

College of Mining, Kunming Metallurgy College, YunNanKunMing, China

Email: 52147319@qq.com

**Abstract.**This paper focuses on beryl mines in the Maji region of Yunnan Province, which are characterized by fluid inclusions. Based on petrography theory, mineralogy, and ore-forming geological conditions, beryl can be divided as $CO_2$ and $CO_2$-$H_2O$ inclusions. In addition, the characteristics of inclusions in the coordinate of A/B is summarized. The homogenization temperature of fluid inclusions in the coordinate of A ranges from 250 °C to 397 °C, while the salinity of fluid inclusions ranges from 0.18% to 4.27%. By contrast, the homogenization temperature in the coordinate of B ranges from 210 °C to 340 °C, and the salinity is from 0.22% to 5.11%. The pressure of ore-forming fluid in the coordinate of A/B is approximately 83 MPa with densities of 0.8034 g/m$^3$ and 0.8363 g/m$^3$, which are characteristic of medium-temperature, low-salinity, and medium-density fluids. Based on Raman spectra and different metallogenic depths, the two types of beryl belong to different metallogenic belts. The beryl deposits in Gongshan are of medium-temperature gas–hydrothermal type.

## 1. Introduction

Beryl (emerald), an ore mineral, is an important refining element of rare metal beryllium. Beryl is also a gem mineral with high economic significance because it contains aquamarine, groups of mother ores, and other types of beryls [1–4]. The metallogenic conditions of beryl are complex. A beryl with different genetic origins or a beryl with the similar genesis but different ore deposits may differ in terms of morphological characteristics and internal structure [5,6]. The special geological conditions of beryls further imply industrial significance because their scales can extend to ore deposits even if their development and utilization are not actively explored. Studies have been conducted on gem and mineral deposits locally and abroad. Gems are considered to be a classic low-temperature high-pressure metamorphic mineral [7,8], which are formed by metamorphic reaction in metamorphic petrology, especially in high-pressure metamorphism [9]. Based on experimental data, different water, temperature, and pressure conditions directly affect melt crystallizations on jadeite. Studies on fluid inclusion highlights the characteristics of metallogenic media obtained during mineral formation (flow and solid) [10-12]. Fluid inclusions are diagenetic ore-forming solutions generated during the growth of mineral crystals, and they are retained when minerals seal the independent closed system boundaries of most crystals. The physical and chemical information of fluid inclusions are then preserved because the newly formed minerals largely represent the original composition of mineral fluids[13-14]. Such processes can describe the genesis and metallogenic geological significance of beryl ores. Fluid inclusions have since been an actively studied field in earth science. Local and international studies of fluid inclusions mainly focus on two aspects: artificial setups and P-T-V-X attributes. In recent years, based on artificial fluid inclusions of $H_2O$-$CO_2$ or $H_2O$-NaCl, two system immiscible research has been one of the important methods for geologists in the exploration of geological function of hydrothermal system fluid process, orogenic belt, and magmatite in the system. Complex three

systems, such as NaCl-$H_2O$-$CO_2$, is also one of the key research objects in years. The influence of fluid composition on the immiscibility of fluid in the three-element system ($H_2O$-NaCl-$CO_2$) has been investigated using the artificial inclusion method. Gibert studied artificial fluid inclusions under high temperature and pressure of the dominant position, where 500– 700 MPa and 900 °C ($H_2O$-NaCl-$CO_2$) were used in the immiscibility system of. Pettke et al. used various components of fluid inclusions in prior artificial control. A comparative analysis of the advantages and disadvantages of different components was conducted; the fluid extraction method of fluid inclusion in the analysis of various processes may influence factor. Researchers have also attempted to use mathematics to process the data obtained from fluid inclusions and analyze the application of various geological information in fluid inclusions using Raman spectroscopy. The equation of state revenue in its MacFlinCor program, which is obtained from the fluid inclusions in data processing and interpretation, can be simplified to facilitate comparison at similar temperature and pressure conditions of inclusion data as suggested by the state equation. Liu Bin studied the characteristics of fluid inclusions in Xinjiang aquamarine and obtained the thermodynamic parameters of mineral formation, thus effectively guiding the synthesis of aquamarine under laboratory conditions. The study of fluid inclusions has also been used to identify days.

The methods for fluid inclusion determination include X-ray diffraction analysis, laser Raman spectrum analysis, infrared optical imaging analysis, scanning electron microscopy (SEM), and energy spectrum analysis. In 1984, Campbell et al. realized the infrared optical imaging study of the internal structure and fluid inclusions of opaque minerals and studied the thermodynamic characteristics of fluid inclusions. A series of opaque and translucent mineral fluid inclusions were measured, including wolframite, enargite, stibnite, hematite and black manganese ore. Additional research on pyrite provides a reference for the study of opaque mineral inclusions. Roedder has been applied to the discovery of chalcopyrite daughter in fluid inclusions in porphyry copper deposits using the SEM technique.

The fluid inclusions widely exist in precious minerals, such as diamond, ruby and sapphire; emerald, aquamarine, olivine, garnet, quartz, tourmaline, Topaz, feldspar, jadeite and nephrite exist in inclusions and a few rare gems according to Li Huishi, who found these minerals in the presence of fluid inclusions. However, compared to the application in other fields, the application of fluid inclusion in gemology has not received sufficient attention. Taking the fluid inclusions in precious jade minerals as the main task, studying the characteristics and causes of jade deposits is a novel idea. The study area of Pula Di Xiang Michel bottom Muscovite mine is located in the county in the south, is the dark horse - Katrina Bay - - sand Gardner Pula bottom Muscovite ore belt of rare metal deposits representative. Owing to the mining area with steep terrain and traffic inconvenience, geological exploration of ore deposit degree is very low.

## 2. Regional geological survey

The mine is located in the eastern Tethys Himalaya tectonic domain, which is lumped between the Gondwana and Eurasian Continental combination zones and has a complex geological structure. This area is mainly dominated by Carboniferous strata. The stony Hanluo-Qide fault can be divided into Mo Xishan District in the east and Nu River District in the west, which is located in the corner of the Pula bottom deposit Mo Carboniferous strata in the north of Xishan district. In addition, this area has frequent magmatic activity, has complex rock type, and its spatial distributions are strictly controlled by regional tectonics. Banded lines are concentrated along the western part of the fault area and are significantly multi-period. The mineralization of Yunnan beryl mine in Gongshan County mainly produce quartz vein, muscovite pegmatite, and Wei Jingyan types containing electrical sodium.

## 3. Geological characteristics of deposits

### *3.1. Mining area*

Mine the main strata with Carboniferous metamorphic Fugong Gongshan: (Cc), on the whole, the upper strata in marble and metamorphic quartz sandstone has sandwiched phyllite; lower phyllite and quartz sandstone are interbedded or granulite schist is interbedded thick. Clip massive quartzite and quartz sand in horizontal and vertical directions are obvious. In the vertical direction, the original rock is a set of marine clastic sedimentary and volcano rock–carbonate rock formation, as well as a prosodic structure of sandstone and mudstone. Frequently, even flysch development reflects the strong oscillatory motion in the transverse direction from south to north, with the metamorphism indicating a gradually shallowing trend in the region, especially in the Pula bottom mining area. The southern extension not only shows the degree of metamorphism but also migmatization deepens and intensifies.

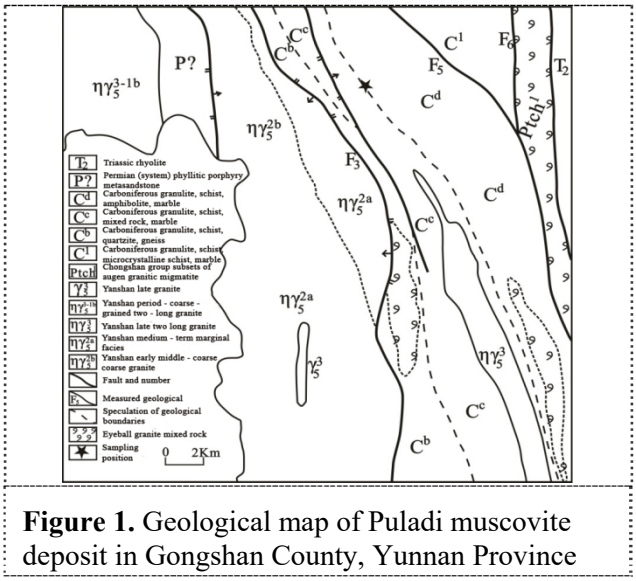


**Figure 1.** Geological map of Puladi muscovite deposit in Gongshan County, Yunnan Province

*3.2. Mine structure*

The tectonic development in the area can be observed near SN, and NNW to SSE is located near the mine. Nujiang Fault passes by the side of the mining area, and the structure of the mining area is controlled. The mining area is located approximately 100 m east of the cross-Golmi Fault, which is a monoclinic structure with NE inclination. The formation of the strata is 50° to 60° ∠ 60° to 70°. In the mining area, the secondary tectonic development is mainly observed in the northwest and northeast parts of the fault along the secondary fault into the quartz, peacock, and long veins. The mining area shows an extensive development of fissure structures, as well as the sporadic development of small ruptures. The fissure structure provide a favorable reservoir space for the veins, which, in turn, serves as transport channels for precipitation and enrichment of rare metals, such as niobium, tantalum, and beryllium.

*3.3. Output characteristics of beryl ore body*

The beryls developed in the mining area are all produced in the Weijingyan vein, which is controlled by the dense contact in the granite body of the inner contact zone. The veins (mineralized body) are extremely developed in the fracture site. Owing to the different characteristics of the surrounding rocks and tectonics, the morphology of the veins also varies (Table 1).

**Table 1.** Statistical characteristics of the beryl-bearing veins.

| Veins/minerals | Output site | Length (m) | Thickness (m) |
|---|---|---|---|
| Single strip; plate and dense array of complex pulse group | Granite fissures and surrounding rock | 100–500 | 2–6 |

| | | | |
|---|---|---|---|
| Convex-like and oblong bead-like veins | Interlayer cracks in contact with schist | 200–300 | 1–20 |
| Irregularly tumor-like cystic veins | Granite contact with the schist | 10–80 | 10–40 |
| “X” cross-shaped and “Ling” reticular complex pulse group | Granite Shear Fracture Development Lot | 100–400 | 1–5 |
| Yoke-curved veins | Rock contact zone | 10–200 | 5–20 |

## 4. Petrography and fluid inclusion body of rock samples

### *4.1. Samples of beryl*

Coordinate A sample: (1) Beryl is colorless with a crude pegmatitic granite texture. Under a microscope, the sample is raised to moderate. In addition, the surface is smooth, but the cleavages appear with longitudinal striation. Orthogonal microscopy showed a level of yellow interference, parallel extinction, positive ductility, and the presence of uniaxial negative crystal.

Coordinate B sample: (1) Beryl is colorless with large crystals, although the shape of the crystal is unclear. The sample shows the development of a group of sparse and incomplete cleavage with positive protrusions. In addition, the surface is generally smooth. The refractive index is relatively high than quartz and muscovite, and an orthogonal next-level dark gray interference color exists. The cone light appears perpendicular to the optical axis with a black cross-interference map and a negative axis crystal.

### *4.2. Petrographic characteristics of inclusions*

The boundary of the inclusions in the berth of coordinate A is clear and transparent, the distribution is mostly dominated by clusters, and the locus appears star-shaped and isolated. The shape of the inclusion mostly appears as an elliptical, elongated, and irregular band. The inclusions in the beryl can be divided into two categories: (1) $H_2O$ inclusions in beryl (40%) with a gas filling concentration at 10%–25% and large sample sizes of approximately 25 μm × 10 μm. (2) Large $CO_2$-$H_2O$ inclusions in the beryls which account for approximately 60% of the samples: liquid-phase $H_2O$, liquid-phase $CO_2$, and gas-phase $CO_2$. The phase filling degrees range from 10% to 50% (Figures 2-a/b), which are elliptical, elongated, irregular, and clustered or crystalline. The shape of the beryl sample from coordinate B is similar to that of coordinate A but the dimensions are different; that is, the sizes of the $H_2O$ inclusions are 40 μm × 10 μm. When the size is 80 μm × 30 μm, the size of $CO_2$-$H_2O$ is 45 μm × 15μm (large ones are 85 μ m × 8μm) (Figures 2-c/d).

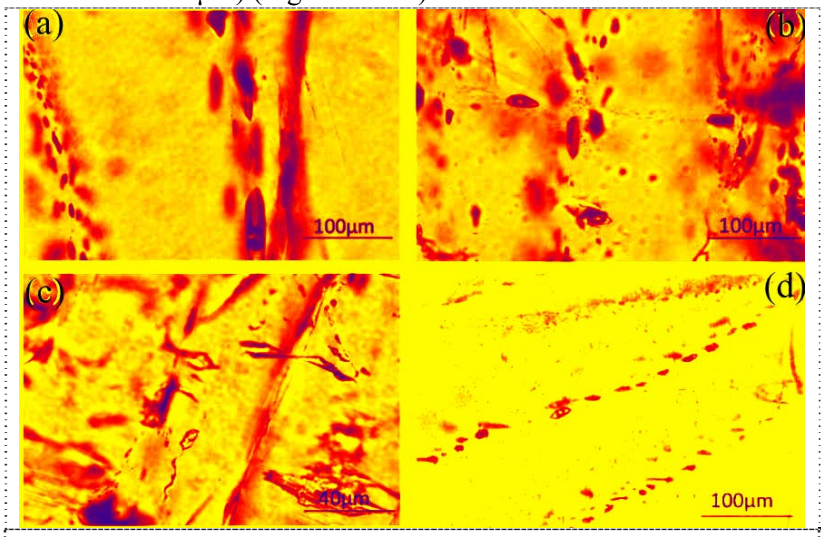


**Figure 2.** Micrograph of coordinate A/B inclusions

## 5. Determination of uniform temperature and salinity of fluid inclusions

### *5.1. Coordinate A uniform temperature and salinity*

At room temperature, the three-phase inclusions in coordinate A contain gas-phase $CO_2$, liquid-phase $CO_2$, and liquid-phase $H_2O$. In the obtained $CO_2$-$H_2O$ inclusions, a typical uniformity of the inclusions was selected, as shown in Figure 3-a. The uniform temperature range of the inclusions was 250 °C to 333 °C, with an average value of 310.54 °C. The temperature of the cage was 11 °C with a temperature range of 8.9 °C to 9.9 °C and an average value of 9.3 °C.

At room temperature, the gas–liquid $H_2O$ inclusions in coordinate A contained $H_2O$ and liquid-phase $H_2O$ with a gas-phase filling degree of approximately 10%. The average temperature of the $H_2O$ inclusions ranged from 288 °C to 397 °C with an average temperature of 337 °C (Figure 3-b). Gas–liquid $H_2O$ was also measured in this experiment. The freezing point of the inclusions ranged from −2.4 °C to −0.1 °C.

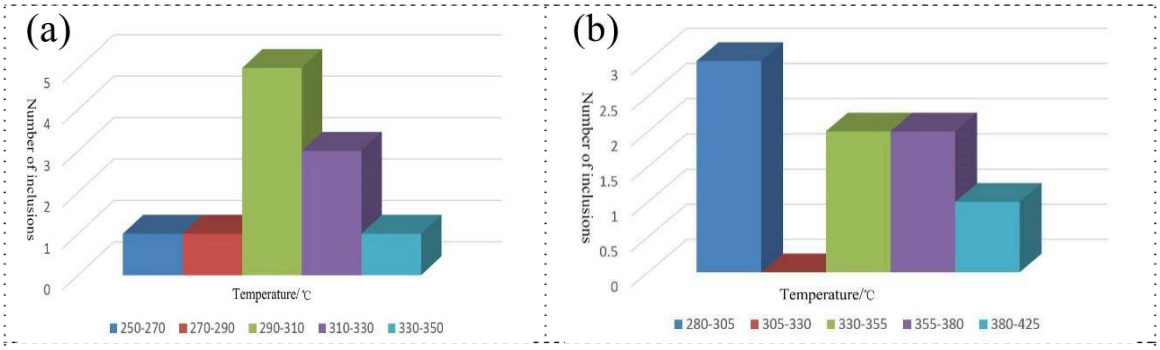


**Figure 3.** Homogenization temperatures of $CO_2$-$H_2O$/$H_2O$ inclusions in coordinate A

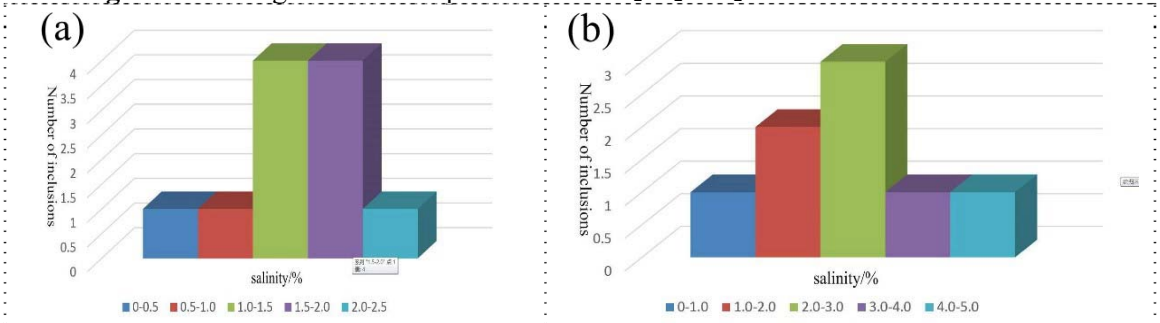


**Figure 4.** Salinity of $CO_2$-$H_2O$/$H_2O$ inclusions in coordinate A

### *5.2. Coordinate B uniformity temperature and salinity*

In this study, representative samples from the $CO_2$-$H_2O$ inclusions are selected to have a uniform temperature of 32 °C, and the uniform temperature of inclusions ranged from 250 °C to 340 °C with an average temperature of 301.39 °C (Figure 5-a). The temperature of the inclusions was 32 °C at the range of 8.3 °C to 9.9 °C with an average of 9.28 °C.

At room temperature, the $H_2O$ inclusions in coordinate B comprised gas-phase and liquid-phase $H_2O$. In this study, the representative inclusions are selected to have a uniform temperature of 14 °C. The temperature range of $H_2O$ wis 210 °C to 321 °C with an average of 254 °C, as shown in Figure 5-b. Meanwhile, the gas–liquid $H_2O$ inclusions obtained a freezing point temperature of 14 °C, and the freezing point temperature ranges from −3.1 °C to −0.2 °C with an average of −1.2 °C.

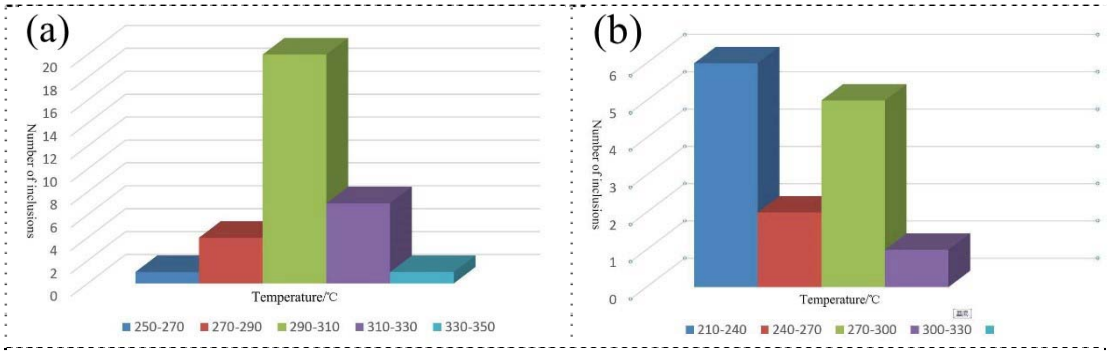


**Figure 5.** Homogenization temperatures of $CO_2$-$H_2O$/$H_2O$ inclusions in coordinate B

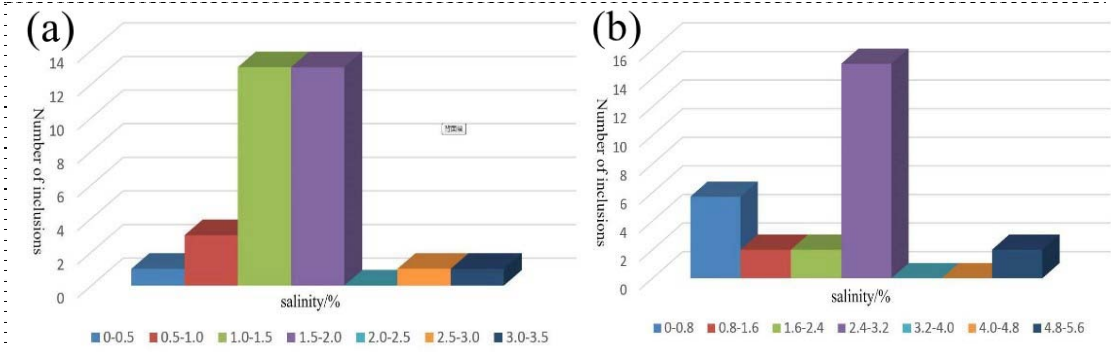


**Figure 6.** Salinity of $CO_2$-$H_2O$/$H_2O$ inclusions in coordinate B

## 6. Fluid inclusions and metallogenic analysis

### *6.1. Fluid inclusion density and pressure*

A temperature, salinity, and density phase diagram shown in Figure 7 is obtained by measuring the freezing point temperature from the freezing stage, combined values of temperature and salinity, and uniform temperature (T) of fluid inclusions in relation to salt (w). The density curve value indicating the intersection of the two vertical lines corresponds to fluid density. On this basis, gas-phase saturation pressure value can be determined by referring to the T- p phase diagram shown in Figure 8 for homogeneous fluids.

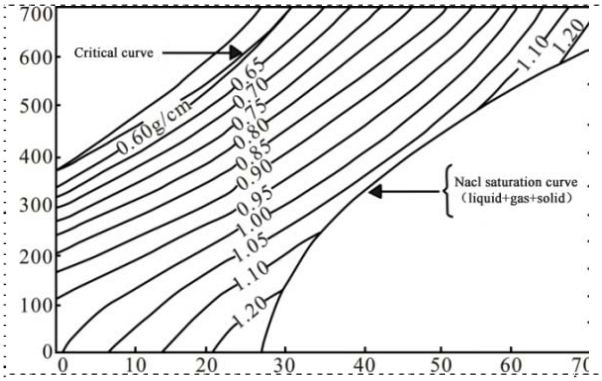


**Figure 7.** Phase diagram of T-W- ρ for NaCl-$H_2O$ system[16].

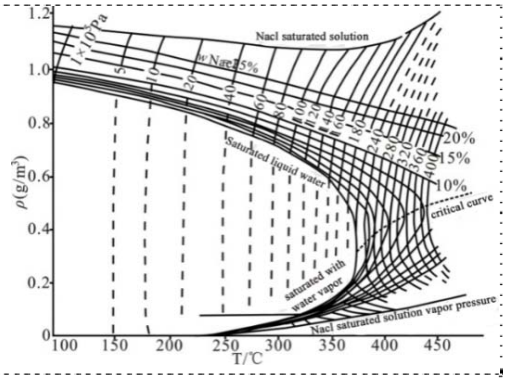


**Figure 8.** Phase diagram of T- ρ for NaCl-$H_2O$ system.

Coordinate A: Based on Figure 4-a and look-up table analysis, the $H_2O$-$CO_2$ inclusions obtained the following: salinity of 0.22%–4.27% with an average of 1.4136%; density of 0.6197 g/m$^3$–0.8034

g/m$^3$ with an average of 0.8034 g/m$^3$; and pressure of 70.4 MPa–99.99 MPa with an average of 83.5645 MPa. In addition, based on Figure 4-b and table analysis, the $H_2O$ inclusions obtained a salinity of 0.18% to 4.03% with an average of 2.22%; fluid density of 0.565 g/m$^3$–0.761 g/m$^3$ with an average of 0.667 g/m$^3$; and pressure of 7.5 MPa–28.5 MPa with an average of 15.55 MPa.

Coordinate B: Based on Figure 6-a and look-up table analysis, the $H_2O$-$CO_2$ inclusions obtained the following: salinity of 0.22% to 3.33% with an average of 1.44%; density of 0.7675 g/m$^3$–0.8770 g/m$^3$ with an average of 0.8363 g/m$^3$; and pressure of 63.4 MPa–106.6 MPa with an average of 88.73 MPa. Average salinity is 2.07%, whereas fluid density concentration ranged from 0.701 g/m$^3$ to 0.875 g/m$^3$ with an average of 0.801 g/m$^3$. Uniform pressure considerably changes and is concentrated at 18 MPa–114 MPa with an average pressure of 39.536 MPa.

*6.2. Mineralization analysis*

From the preceding estimates of salinity and density results of $CO_2$-$H_2O$ inclusions, the low values for overall salinity in the mining area indicate an overall low-salinity system of fluid inclusions. Moreover, density is classified as medium density, the ore-forming fluid showed low-salt and medium-density characteristics, composite beryl inclusions appeared general characteristics. The average temperature and pressure of the $CO_2$-$H_2O$ inclusions in coordinates A and B, as well as their average fluid densities, are similar except for the minimum value of fluid density, thereby indicating that the two areas are wrapped. Hence, the body may not belong to the same ore belt. Figure 9 shows that the symmetry stretching and vibration peaks of the beryls in different sampling zones, as well as the Raman spectra, vary. The beryl structure in coordinate A is a complex water structure, while the Raman peak relief in coordinate B is weak. The shifting of -O-H and Raman vibration peaks indicate a high water ratio, which further imply that the two sampling areas are rich in water and may belong to different metallogenic batches .

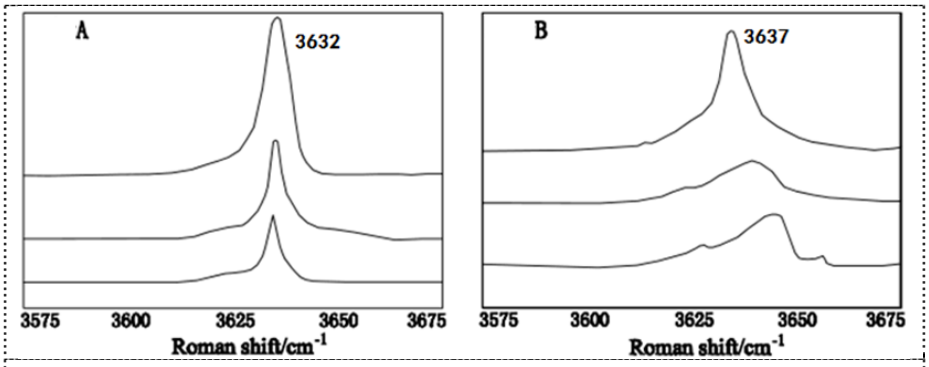


**Figure 9.** Roman spectra of beryl in different coordinates

The mineralization depth of beryl in coordinate A/B is calculated using the static rock pressure formula ($P = \rho gh$, where $\rho$ is the average surface density of the crust surface covering 2.75 g/cm$^3$) to further verify metallogenic regularity. In the pressure values of column A, the average pressure is 83.5645 MPa, and the mineralization depth of $CO_2$-$H_2O$ inclusions is approximately 3.1 Km. Meanwhile, the pressure of the coordinates of beryl in column B is 63.4 MPa–106.6 MPa (average: 88.377 MPa), and the mineralization depth of the $CO_2$-$H_2O$ inclusions is 3.3 Km. In addition, based on the average homogeneous temperatures (Figures 3-b and 5-b) of the $H_2O$ inclusions measured in the two coordinates and their average salinity difference (Figures 4-b and 6-b), the corresponding mean uniform pressure values are 15.55 MPa and 39.536 MPa. A considerable difference exists in metallogenic pressure, which indicates that beryllium is different in the coordinate system.

## 7. Conclusion

The granite mineralization in the study area is controlled by geological factors, such as stratigraphy, magma, and structure. The exposed Carboniferous stratigraphy of the mining area and the secondary tectonic development of the Fugong-Gongshan Metamorphic Belt provide favorable migration channel and ore storage space for the mineralization hydrothermal system. Mineralization is developed in the muscovite, which can be divided into mica belt, quartz–beryl enrichment zone, and albite metasomatic belt.

The beryl is light green to yellowish green and mostly translucent; its crystals are hexagonal and cylindrical and are partly wedged. Mineralization and muscovite formation are similar and continuous, but mineralization is more stable than the latter.

The beryl fluid inclusions in the region are mainly $CO_2$ pure inclusions and $H_2O$-$CO_2$ inclusions, in which $H_2O$ inclusions are 40% in beryl while gas filling is 10% to 25%. However, $CO_2$-$H_2O$ in beryls are more developed than $CO_2$ pure inclusions and account for 60% of the inclusions. Three types of inclusions are distinguishable in room temperature: liquid phase $H_2O$, liquid phase $CO_2$, and gas phase $CO_2$.

The fluid inclusions are measured by using the quenching method and with a Lei heating station in hot and cold tables. The result showed the following: the uniform temperature of the $CO_2$-$H_2O$ inclusions is 250 °C–333 °C; the corresponding salinity is 0.22%–4.27%; density is 0.6197 g/m$^3$–0.8477 g/m$^3$; and pressure is 70.4 MPa–99.99 MPa.

The number of different position coordinates from the Raman spectroscopy test results indicate that various beryl areas and Raman displacement differ, thereby showing different batches of ore, ore-forming pressures,and ore-forming depths. $CO_2$-$H_2O$ and $H_2O$ inclusions, homogenization temperature, and salinity calculations are necessary to further verify whether the areas belong to two different mineralization metallogenic belts.

## References

[1] Li J, Wang L J, Wang L Z, Zhang C J, Shi Y J, Chen Y and Li J L 2012. *Mineral Resources*.32 (4): 563-568.
[2] Yu X Y, Li J P, Wang L Luo W D, Shi Y J, Chen Y and Chen J H 2011. *China mining*.,20 (11): 61-63.
[3] Ren W, Wang L Z, and Li J P 2009. *Mineral Resources*. (S1): 458.
[4] Chang H L, Wang X W, Wang X D, Liu J P and Huang H L 2007. *Journal of Rock and Mineralogy*.26 (3): 259-268.
[5] Ruan Q F, Zhang L G, Zhang C L, Lei W, Rao C, Liao B L and Zeng W L 2008. *Mineral Resources and Geology*.22 (3): 265-269.
[6] Pei J C and Zhang H K. *Geological Science and Technology Information.* 19 (1): 32-34.
[7] Miyashiro, A. 1994. *Metamorphic petrology*. CRC PressI Llc.
[8] Shigeno, M., Y. Mori, and T. Nishiyama 2005 Kyushu Japan. *Journal of mineralogical and petrological sciences*. 100(6): p. 237-246.
[9] Boettcher, A. and P. Wyllie 1969. *American journal of science*. 267(8): p. 875-909.
[10] Deng J S, Wen S M, Wu D D, Liu J, Zhang X L and Shen H Y 2013. *International Journal of Minerals, Metallurgy, and Materials*. 20(9): p. 815-822.
[11] Deng J S, Wen S M, Liu J, Xian Y J, Wu D D and Bai S J 2013. *Industrial & Engineering Chemistry Research*. 52: p. 4895–4901.
[12] Deng J S, Wen S M, Xian Y J, Liu J and Bai S J 2014. *Transactions of Nonferrous Metals Society of China*. 24: 3955–3963.
[13] Deng J S, Wen S M, Xian Y J, Liu J and Bai S J 2013.*Minerals Engineering*.42: 22–28.
[14] Deng J S, Mao Y B, Wen S M, Xian Y J and Liu J 2015. *International Journal of Minerals, Metallurgy and Materials*. 22: 111–116.
[15] nd C.M. Graham 1999.*Contributions to mineralogy and petrology*.136(3): p. 247-257.
[16] Brown, P.E. and S.G. Hagemann 1994. *Blacksburg VA, Virginia Polytechnic Institute and State University.* p. 231-250.